Applied Physics Letters

Efficient terahertz radiation absorption by dilute graphene composites

Cite as: Appl. Phys. Lett. **120**, 063104 (2022); https://doi.org/10.1063/5.0079891
Submitted: 25 November 2021 • Accepted: 27 January 2022 • Published Online: 09 February 2022

Zahra Barani, Kamil Stelmaszczyk, Fariborz Kargar, et al.

Applied Physics Letters ARTICLE scitation.org/journal/apl

Efficient terahertz radiation absorption by dilute graphene composites

Cite as: Appl. Phys. Lett. **120**, 063104 (2022); doi: 10.1063/5.0079891
Submitted: 25 November 2021 · Accepted: 27 January 2022 ·
Published Online: 9 February 2022

Zahra Barani,[1,2] Kamil Stelmaszczyk,[3] Fariborz Kargar,[1,2,a)] Yevhen Yashchyshyn,[3,4] Grzegorz Cywiński,[3] Sergey Rumyantsev,[3] and Alexander A. Balandin[1,2,a)]

AFFILIATIONS

[1]Nano-Device Laboratory, Department of Electrical and Computer Engineering, University of California, Riverside, California 92521, USA
[2]Phonon Optimized Engineered Materials Center, University of California, Riverside, California 92521, USA
[3]CENTERA Laboratories, Institute of High-Pressure Physics, Polish Academy of Sciences, Warsaw 01-142, Poland
[4]Institute of Radioelectronics and Multimedia Technology, Warsaw University of Technology, Warsaw 00-665, Poland

[a)]**Authors to whom correspondence should be addressed:** fkargar@ece.ucr.edu and balandin@ece.ucr.edu.
URL: http://balandingroup.ucr.edu/

ABSTRACT

The interaction of terahertz electromagnetic radiation with dilute graphene-epoxy composites was studied experimentally at frequencies from 0.25 to 4 THz. Composites with low graphene loading ($\leq$1.2 wt. %) below the electrical percolation threshold revealed the total shielding effectiveness above ~70 dB (1 mm thickness) at 1.6 THz frequency. The unexpected high shielding effectiveness of dilute graphene composites in blocking terahertz radiation was mostly achieved by absorption rather than reflection. The shielding effectiveness increases with increasing frequency. Our results suggest that even the thin-film or spray coatings of the lightweight, electrically insulating graphene composites with thicknesses in the few-hundred-micrometer range can be sufficient for blocking terahertz radiation in many practical applications.

Shielding of electromagnetic (EM) energy in the terahertz (THz) frequency range is important for both reducing EM interference among various devices and protecting humans.[1–3] While efficient THz sources are still under development, electromagnetic interference (EMI) shielding approaches for the relevant frequency band have already attracted significant attention.[4,5] Absorbing EM radiation in the THz band and, simultaneously, meeting all practical constraints can be challenging. There are numerous requirements imposed on materials used for EM interference (EMI) shielding such as the thickness of the coating layer, weight limits, mechanical and thermal properties, electrical isolation or conductance, reliability, and cost. Absorbing EM energy rather than reflecting it back to the environment is often required for commercial, e.g., 6G technology, and defense applications.[6] Many existing EMI shielding materials for high-frequency bands, including metallic coatings, mostly redirect the EM energy by reflection owing to their high electrical conductivity. Reflection protects electronic components but, at the same time, may negatively affect human health.[2,3]

An alternative promising approach for EMI shielding is the use of polymer-based materials with electrically conductive fillers.[7–9] Recent studies reported the use of carbon fibers,[10,11] carbon black,[11,12] bulk graphite,[13,14] carbon nanotubes,[15–18] reduced graphene oxide,[19–24] graphene,[25,26] and a combination of carbon allotropes with other particles.[24,26–29] Graphene was used successfully as the filler in composites, which were tested in the MHz and GHz frequency ranges.[22,26,30,31] There were a few reports on the use of graphene composites in the subterahertz and THz range.[32–35] Experimental and theoretical studies with individual graphene layers and graphene meta-surfaces suggest that graphene interacts efficiently with EM radiation in the THz range.[36–40] Available data suggest that graphene particularly absorbs radiation well in the high GHz frequency range rather than reflecting it back to the surroundings.[33] Further work is needed to understand EM characteristics of such composites at different loading of graphene and assess their application potential.

In this Letter, we report the results of testing of composites with epoxy base and low loadings of graphene below 1.2 wt. %. The term

graphene, in the context of composite studies, is used to identify a mixture of graphene and few-layer graphene (FLG) with micrometer-scale lateral dimensions. For this study, we utilized FLG powder (xGnP®H-25, XG-Sciences, USA) as a starting material to prepare the composites. The as-synthesized FLG flakes have the average lateral dimensions in the range from 15 to 25 μm, an average FLG thickness of ~15 nm, and a typical surface-area-to-mass ratio of 50–80 m^2/g. It should be noted that the actual thickness of the graphene fillers in the composite is less due to further exfoliation during composite preparation, which includes the use of the high-shear mixer. The "bulk" in-plane and cross-of-plane electrical conductivity of the graphene flakes are up to $\sim 10^7$ and $\sim 10^2$ S/m, respectively. We found the optimum exfoliation and shear mixing parameters via extensive trial-and-error effort. A particular emphasis was on obtaining a uniform dispersion of graphene fillers. The samples were prepared in the form of disks with a diameter of 25.6 mm and thicknesses varying from 0.9 to 1.0 mm. The quality of the dilute graphene composites was verified using scanning electron microscopy (SEM) and Raman spectroscopy. The details of the composite synthesis and material characterization data are provided in the supplementary material.

The EMI shielding effectiveness of the dilute graphene composites was investigated using the terahertz-time domain spectroscopy (THz-TDS) system (Toptica Photonics AG).[41–43] A train of short THz pulses of ~1 ps duration and the repetition rate of 100 MHz was sent through the sample pellets made of the composites or was reflected from their surfaces depending on the experimental geometry. The high-mobility InGaAs photoconductive antennas were used as both a transmitter (Tx) and a receiver (Rx). The antennas were fed with an all-fiber pulsed laser centered at 1.56 μm wavelength. As opposed to 1 ps duration of the THz pulses, the duration of the laser pulses was much shorter, $\tau \sim 80 f$s. Owing to this property, a time narrow fraction of the THz pulse could be sampled at one given delay of the laser pulse. To retrieve temporal profiles of the pulses from the THz pulse train, a variable delay stage scanned the THz wave packet with the laser probe pulse. The high repetition rate of the pulse train allowed us to obtain effective wave packets sampling at the rate of ~30 traces/s and to average over 1000–2000 pulses during a single minute duration of an individual measurement. A fast Fourier transform (FFT) algorithm was used to calculate the amplitudes and phases of the transmitted and reflected fields as a function of frequency.

A schematic of the THz-TDS experimental setup is shown in Fig. 1. In addition to the laser part, it includes the THz beam delivery part based on the so-called 4f optical arrangement,[44] consisting of four 90° off-axis parabolic mirrors. The two of these mirrors, applied to compensate for the divergence of the beam, were located, after the transmitter and, after the sample. The other two provided focusing before the pellet and detector. The focal lengths of the mirrors were chosen to ensure symmetrical propagation of the beam on the distance from the radiation source to the sample and from the sample to the detector. The diameter of all mirrors was 25.4 mm, and the shorter and longer focal lengths were 50.8 and 101.6 mm, respectively. Using these values, one can estimate that the Rayleigh lengths $z_R = \pi\omega_0^2/\lambda$ (ω_0 is the beam waist in focus, and $\lambda = c/f$, where c is the speed of light and f is the radiation frequency) of the pulse frequency components (0.25–4.0 THz) were not shorter than ~1.5 mm, i.e., sufficiently longer than the thickness of the composite pellet. Such a situation typically indicates good collimation of the beam near the focal spot, providing equal absorption lengths for all frequency components. Note that the setup shown in Fig. 1 was used only for the measurements of the transmission coefficients, T. To measure the reflection coefficients, R, the receiver was placed on the same side of the sample as the transmitter, and the amplitude of EM radiation reflected from the surface of the pellet was measured. Special care was taken to deliver the beam at nearly normal incidence with respect to the sample, resulting in a small deviation of only 4° from the vertical.

A procedure involving measurements of the transmission, T, and reflection, R, coefficients commonly used in the S-matrix method[16] was applied to determine the absorption properties of composites.

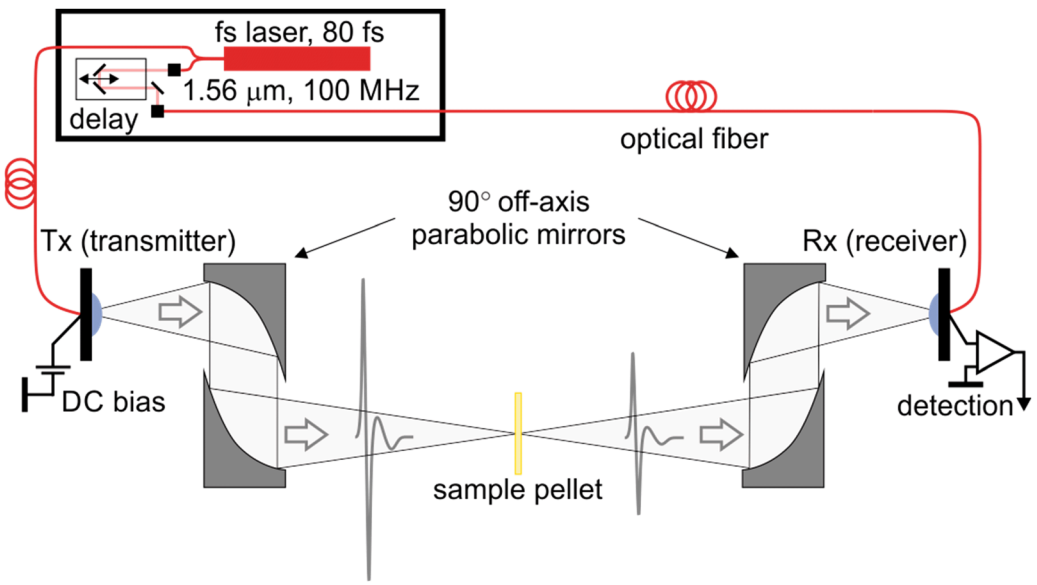

FIG. 1. Schematic of the experimental setup used for the measurements in the high-frequency range from 0.25 to 4.0 THz.

The transmission coefficient of composites was calculated by measuring the amplitude of the electric field transmitted through the sample, $\hat{E}_{21s}$, and through the reference field, $\hat{E}_{21e}$. The latter was measured in an empty space after removal of the composite. On the basis of these two measurements, T was calculated as

$$T = |S_{21}|^2 = \left|\hat{E}_{21s}/\hat{E}_{21e}\right|^2. \quad (1)$$

Similarly, the reflection coefficient was determined by measuring the electric field, $\hat{E}_{11s}$, reflected from the surface of the epoxy composite. The reference field, $\hat{E}_{11s}$, was measured with the THz pulse reflected from the polished metallic plate, which is a good approximate of an ideal reflector in the THz band. An equivalent of Eq. (1) was used to calculate R as follows:

$$R = |S_{11}|^2 = \left|\hat{E}_{11s}/\hat{E}_{11m}\right|^2. \quad (2)$$

The electric fields from Eqs. (1) and (2) and the phase relations required to calculate the amplitude ratios were provided by the FFT. Finally, to determine the absorption characteristics of an EMI shielding material, the measured values of T and R were used to calculate the effective absorption coefficient, A_{eff}, defined as

$$A_{eff} = (1 - R - T)/(1 - R). \quad (3)$$

Compared with the standard definition of the absorption coefficient $A = 1 - R - T$, the modified definition describes the actual absorption of the composite material accounting for the fact that some part of the incident EM energy is always reflected from the surface of the sample. The total shielding effectiveness, SE_T, shielding via different mechanisms of reflection, SE_R, and absorption, SE_A, can be calculated knowing R and A_{eff} as follows:[33]

$$SE_R = -10\log(1 - R), \quad (4)$$

$$SE_A = -10\log(1 - A_{eff}), \quad (5)$$

$$SE_T = SE_R + SE_A. \quad (6)$$

Figure 2(a) shows the reflection coefficient, R, for the pristine epoxy and three epoxy-based composites with the graphene loading ranging from 0.8 to 1.2 wt. %. The data are presented in the frequency range from 0.25 to 4 THz. The oscillations of the reflectivity at low frequencies are due to the multiple reflections from the sample's front and back surfaces, causing Fabry–Pérot interference features. The sharp spikes at $f > 1.5$ THz are due to the absorption by the water molecules in the atmosphere. Within the whole frequency range, the reflection from the epoxy-based composites is small. Figure 2(b) presents the reflection shielding effectiveness of samples as a function of frequency. One can see that shielding by reflection in the whole frequency range is below 1 dB.

The transmission coefficient, T, for the same set of samples is shown in Fig. 3(a). It is interesting to note that the transmission decreases with increasing frequency. For composites with a graphene loading of 1.2 wt. %, and at $f = 1.6$ THz, $T \sim 10^{-7}$%, confirming that almost all the incident EM wave is blocked by the composites. This level of the measured signal is already close to the sensitivity limit of the measurements. As expected, the higher the graphene loading, the smaller is the transmission. The exception is only observed at the frequencies below $f = 0.4$ THz, where the transmission spectra for the composites with 1.0 and 1.2 wt. % loading of graphene coincide.

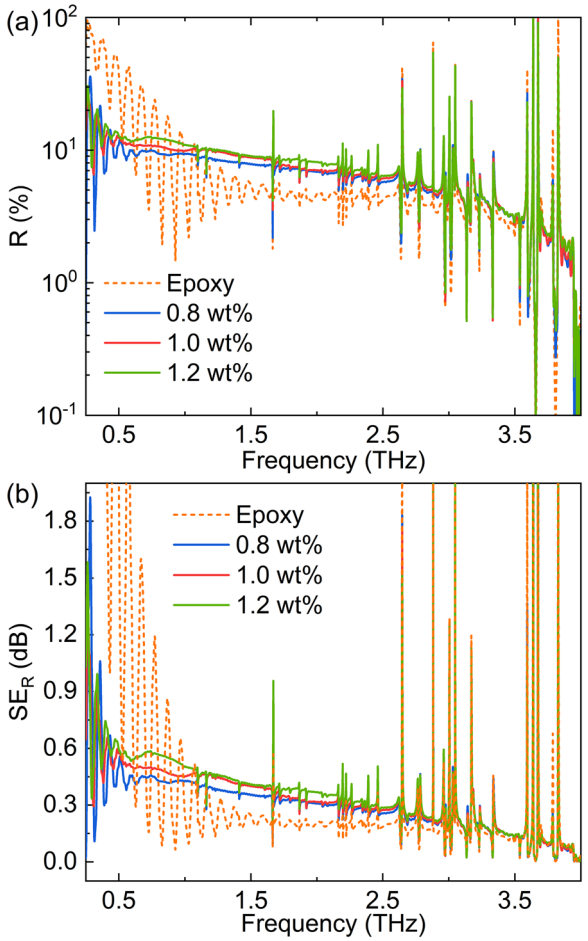

FIG. 2. (a) Reflection coefficient, R, and (b) reflection shielding effectiveness, SE_R, of the pristine epoxy and the composites with low loadings of graphene as a function of frequency. Note that the shielding by reflection is negligible in all composites. The experiments have been conducted using an aluminum plate as a reference.

The low reflection and low transmission of the epoxy-based composites in the THz frequency band show that this material effectively shields EM radiation mainly due to absorption. It is important to note that our dilute graphene composites are electrically insulating, and their resistivity could not be measured by a standard four-probe measurement setup. Our previous studies with the same polymer and graphene fillers have shown that the electrical percolation occurs at ~5 wt. % of the filler loading.[33] This is a loading fraction required for graphene fillers to physically touch each other and form a conductive path. The dashed lines in Fig. 3(a) show the result of recalculation of the experimental data for a 1-mm thick sample to the thickness of 200 μm. Given that most of the loss is caused by the absorption mechanism (i.e., $SE_R < 1$ dB), we used the Beer–Lambert law to extrapolate the transmission and total shielding effectiveness in thinner samples. It is seen that even these thin layers can protect effectively at the THz frequency band. The total shielding effectiveness of the dilute graphene composites, SE_T, is presented in Fig. 3(b). One can see that 1.2 wt. % graphene composites provide total shielding above ~70 dB at

$f \sim 1.6$ THz, which is more than sufficient for many industrial applications. Multiple reflections have not been observed in our dilute graphene samples above 0.25 THz owing to the strong absorption. The latter was verified from the analysis of the delayed pulses, following the first transmitted pulse. Such pulses give rise to distinguishable Fabry–Pérot interference patterns in the measured spectra, for example, of the pristine epoxy, which has low absorption.

The frequency dependence of A_{eff} and SE_A are shown in Figs. 4(a) and 4(b), respectively. The data demonstrate conclusively that absorption is the dominant mechanism for blocking the EM waves in our dilute graphene polymer composites. One can see that especially at frequencies $f > 0.6$ THz, these composites absorb EM radiation almost completely. The composites with 1.2 wt. % of graphene loading provide ~45 and ~80 dB shielding effectiveness by absorption at $f \sim 0.8$ THz and $f = 1.6$ THz, respectively [Fig. 4(b)]. These samples reveal substantially higher absorption shielding effectiveness compared to PDMS composites with 3 wt. % graphene content in the near-THz frequency range.[32]

At this point, the physical mechanism of THz absorption in dilute graphene composites can be analyzed only qualitatively. We start with comments on the intrinsic properties of graphene fillers. The electrical conductivity of graphene is a strong function of the carrier concentration, e.g., the Fermi level position, which can change over a wide range. Unlike individual graphene devices,[45] where gating defines the Fermi level position, the conductivity of graphene fillers in composites is determined by the "chemical doping" from the base material. It is not possible to determine exactly the electrical conductivity of graphene fillers inside the matrix. Typical values of the in-plane electrical conductivity reported for large layers of chemical vapor deposition (CVD) grown graphene are in the range of 10^3–10^6 S/cm.[46,47] The sheet resistance for CVD graphene was reported to be in the range of 100–300 Ω/sq.[48] The "chemical doping" inside the base materials, defects, and disorder can change the electrical conductivity in a wide range of values. In terms of the electrical conductivity, graphene fillers are similar to metal fillers although extremely thin ones. The EM absorption of graphene is known to have a peak at 4.62 eV related to the many-body interactions, i.e., excitons.[49] However, in the context of THz absorption in composites, more important is the high aspect ratio of the fillers, their size, and distributed nature of the scatterers.

A recent study proposed a physical model based on the Maxwell–Garnett theory for the complex dielectric permittivity of composites.[5] The model was written in terms of the polarizability of inclusions, suitable for nanoscale carbon fillers. The agglomerates and connected fillers were considered as structures with higher aspect ratio and lower effective conductivity. The effective conductivity decreases due to the presence of contact resistances between the fillers. The model was tested on polylactic acid composites with graphite nanoplates.[5] The model predicts a peak in the absorption in the relevant frequency range from high-GHz to several THz depending on the main parameters—aspect ratio, size, and electrical conductivity of the fillers. Our experimental results are in line with this Maxwell–Garnett-based model, and the absorption spectra can be reproduced by fitting the aspect ratio and electrical conductivity of the fillers within a reasonable range.

Another phenomenon, which may affect the EM energy absorption in dilute graphene composites is the filler–matrix interaction.

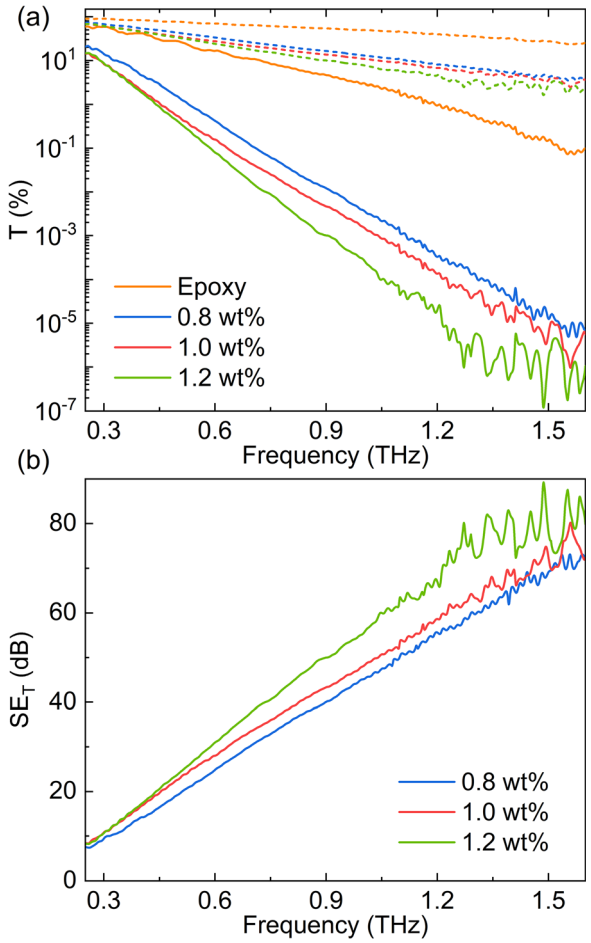

FIG. 3. (a) Transmission coefficient, T, and (b) total shielding effectiveness, SE_T of the composites with low loadings of graphene as a function of frequency. Note that SE_T increases linearly with the frequency. For $f \geq 1.6$ THz, the shielding effectiveness of the dilute graphene composites increases beyond the measurable upper limit of the instrument. The solid lines are the experimental results for samples with 1 mm thickness. The dashed lines in panel (a) are the calculated T and SE_T for 200 μm thick samples, provided for comparison. Note the change in the slopes of the curves at $f = 0.4$ THz.

It was recently reported that polyethylene with graphite particles (2.5 wt. % loading) reveals a strong attenuation, i.e., absorption, peak at ~2.2 THz.[35] The authors attributed this attenuation peak to graphite particles' interaction with the matrix or the presence of impurities in the sample. At higher frequencies, there was a monotonic growth of the attenuation with frequency increase that was explained by the Rayleigh scattering. The absorption mechanism related to the graphene–matrix interaction was proposed in another study focused on the absorptive properties of graphene composites in the near-THz frequency range. They were explained by the activation of the interaction of atomic vibrations of the polymer matrix with the π-band to polaron band transitions in graphene in the THz frequency range.[50,51] This transition, which is in resonance with THz radiation, can cause strong absorptive properties, yielding a significant THz-range EMI shielding behavior.[50]

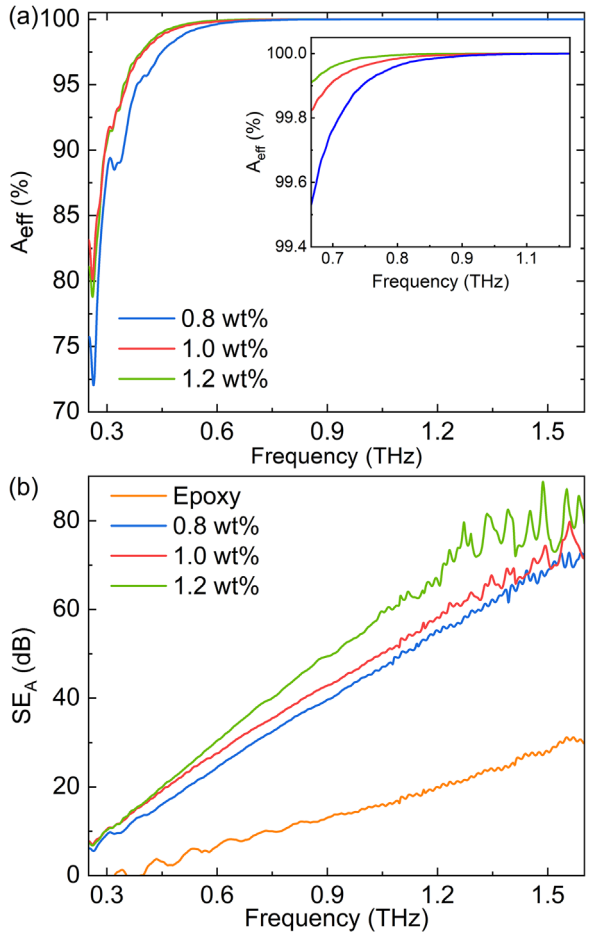

FIG. 4. (a) Effective absorption coefficient, A_{eff}, of the epoxy composites with graphene as a function of frequency. The inset in (a) shows the same graph in the frequency range of 0.6 THz $\leq f \leq$ 1.2 THz. Note that at frequencies $f \geq$ 0.95 THz, the effective absorption reaches ~100%, indicating that the remaining fraction of the incident EM waves after reflection at the interface is completely absorbed by the composites. (b) Frequency-dependent shielding effectiveness of the composites by the absorption, SE_A.

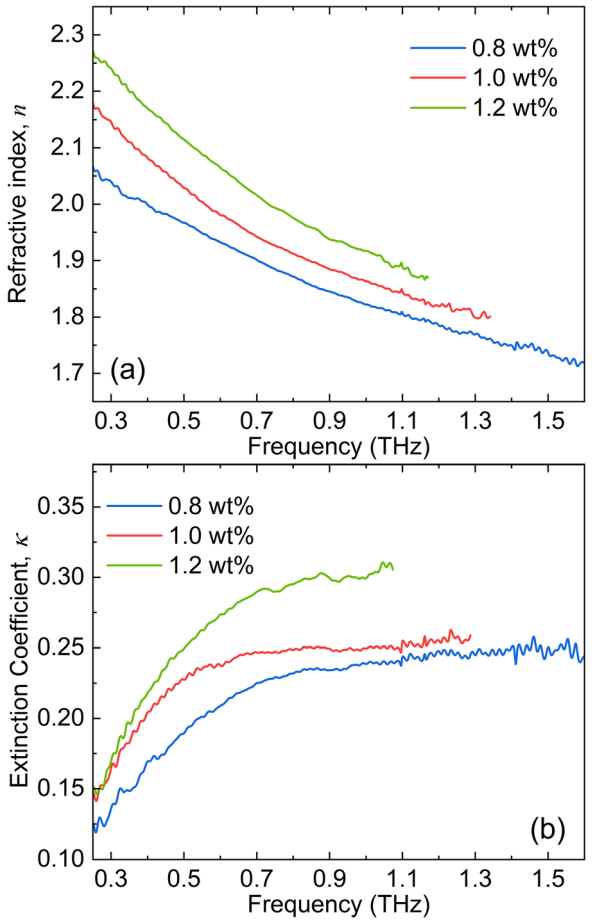

FIG. 5. The complex index of refraction of the dilute graphene composites: (a) index of refraction, n, and (b) extinction coefficient, κ.

There is an additional interesting observation, which can be made from data presented in Figs. 3 and 4. The slopes and the values of the transmission coefficient, T, and the shielding effectiveness, SE_T, are nearly the same for the composites containing 1.0 and 1.2 wt. % graphene at the frequencies below $f = 0.4$ THz (see Fig. 3). On the other hand, the slopes of SE_T curves corresponding to the samples containing 1.0 and 0.8 wt. % of graphene are the same for the frequencies $f > 0.4$ THz. There is a change in the slope, specifically for the dilute composite with 1.0 wt. % of graphene, which happens at $f = 0.4$ THz. A similar trend can be observed for the curves representing the shielding effectiveness related to the absorption, SE_A (see Fig. 4). The slope of the SE_A curve is typically a good estimate of the high-frequency resistivity component of the composite material, ρ.[33,52] We speculate that in this dilute composite, the displacement current, J_D, between graphene fillers separated by an insulating epoxy becomes significant, resulting in the changed characteristics. Since the displacement current density increases with frequency, this assumption should be valid for our electrically insulating samples. To facilitate the use of our experimental data for comparison with other materials, in Figs. 5(a) and 5(b), we present the complex index of refraction, $n+i\kappa$, of our samples. The real and imaginary components, n and κ, were calculated from the magnitude and phase of the scattering parameters, S_{ij}, obtained in the TDS measurements.

We now turn to the applied aspect of the obtained results. The THz absorption shielding characteristics of the dilute graphene composites surpass most conventional polymeric composites with high loading of ceramic fillers such as $BaTiO_3$ or Mxenes.[53] Ceramic fillers are usually used in composites to enhance the absorption component of total shielding. The demonstrated electrically insulating composites can be used as adhesives and environment protective layers for electronic components without shortening them. Such graphene composite absorbers with small thicknesses can be deposited as a protective paint, e.g., spray coatings. Shielding by absorption is crucial in many applications where the EM reflection is undesired. The dilute graphene composites have other advantages compared to various materials recently tested for THz shielding applications.[54] Alternative THz shielding materials include polyacrylonitrile—$Ti_3C_2T_x$ MXene—silver

nanoparticle fiber membranes with different silver nanoparticle contents and thicknesses of porous structures. The reported shielding effectiveness of such fiber membranes with silver nanoparticles reaches up to 12 dB in the 0.2–1.6 THz range.[54] Another study reported the THz shielding performance of the few-layer borophene.[55] The maximum THz shielding effectiveness of borophene-based materials reached up to 50 and 21.5 dB for the reflection loss value in the examined frequency range from 0.1 to 2.7 THz. Most of the shielding reported in Ref. 55 was achieved via reflection. Our dilute graphene composites have the benefit of being prepared from the "generic" graphene without surface functionalization or complicated processing steps. Graphene can be mass-produced via the liquid-phase exfoliation (LPE) or graphene oxide (GO) reduction process.[56–58] Such graphene fillers are inherently better than metals owing to their low cost, absence of corrosion, and high aspect ratio allowing for higher THz absorption.

In this work, the EMI shielding was demonstrated for low power levels. The question of the dissipation of high-power THz energy is an interesting separate problem. Since energy is transferred to heat, there is a limit to the dissipated power because epoxy can withstand a maximum of 150–200 °C. For the majority of applications, e.g., communication, security screening, which deal with small radiation power, the heating of the composite is negligible. If one needs to handle high-power levels, one would need composites with higher loading of graphene. Graphene and FLG have exceptionally high intrinsic thermal conductivity, which can become important if higher graphene loading layers are used together with the electrically insulating dilute graphene layers.[59] In addition to EMI shielding, high-loading graphene composites can dissipate the heat well.[59] Some of us have previously reported the thermal conductivity of epoxy composites with graphene and copper nanoparticles close to 15 W/mK.[60]

In conclusion, we have demonstrated that dilute graphene composites with the low loading of graphene, below 1.2 wt. %, are efficient as electromagnetic absorbers in the THz frequency range. The THz radiation is mostly blocked by absorption rather than reflection. This is different from many other materials and composites used for EMI shielding where reflection is the dominant mechanism for blocking EM waves. The efficiency of the THz radiation shielding by the lightweight, electrically insulating composites, increases with increasing frequency. We argue that even the thin-film or spray coatings of graphene composites with the thickness in the few-hundred-micrometer range can be sufficient for blocking THz radiation in many practical applications.

See the supplementary material for details of composite preparation; optical, SEM, and Raman characterization of the composites; dynamic range of TDS measurements; and calculation of the complex index of refraction.

The work at UC Riverside was supported, in part, by the Office of Technology Partnerships (OTP), University of California via the Proof of Concept (POC) project "Graphene Thermal Interface Materials." This work was also supported by CENTERA Laboratories in frame of the International Research Agendas program for the Foundation for Polish Sciences co-financed by the European Union under the European Regional Development Fund (No. MAB/2018/9).

AUTHOR DECLARATIONS

Conflict of Interest

The authors declare no conflicts of interest.

Author Contributions

A.A.B. and S.R. conceived the idea of the study, coordinated the project, and contributed to the EM data analysis. Z.B. prepared the composites, performed materials characterization, and assisted with the EM data analysis. K.S. and Y.Y. performed the EM shielding measurements and contributed to data analysis. F.K. contributed to the sample preparation and EM data analysis. All authors contributed to writing and editing of the manuscript. Z.B. and K.S. contributed equally to the work.

DATA AVAILABILITY

The data that support the findings of this study are available within the article and its supplementary material.

REFERENCES

[1]M. A. Seo, J. H. Yim, Y. H. Ahn, F. Rotermund, D. S. Kim, S. Lee, and H. Lim, Appl. Phys. Lett. **93**, 231905 (2008).
[2]F. Deruelle, Electromagn. Biol. Med. **39**, 166 (2020).
[3]R. N. Kostoff, P. Heroux, M. Aschner, and A. Tsatsakis, Toxicol. Lett. **323**, 35 (2020).
[4]J. Pan, H. Hu, Z. Li, J. Mu, Y. Cai, and H. Zhu, Nanoscale Adv. **3**, 1515 (2021).
[5]D. Bychanok, P. Angelova, A. Paddubskaya, D. Meisak, L. Shashkova, M. Demidenko, A. Plyushch, E. Ivanov, R. Krastev, R. Kotsilkova, F. Y. Ogrin, and P. Kuzhir, J. Phys. D: Appl. Phys. **51**, 145307 (2018).
[6]G. Li, N. Amer, H. A. Hafez, S. Huang, D. Turchinovich, V. N. Mochalin, F. A. Hegmann, and L. V. Titova, Nano Lett. **20**, 636 (2020).
[7]Z. Tu, Z. Ma, J. Li, J. Liang, S. Li, Y. Shi, and L. Pan, Appl. Phys. Lett. **119**, 150504 (2021).
[8]D. Wanasinghe, F. Aslani, G. Ma, and D. Habibi, Nanomaterials **10**, 541 (2020).
[9]Z. Barani, F. Kargar, Y. Ghafouri, S. Ghosh, K. Godziszewski, S. Baraghani, Y. Yashchyshyn, G. Cywiński, S. Rumyantsev, T. T. Salguero, and A. A. Balandin, Adv. Mater. **33**, 2007286 (2021).
[10]J. Wu, Z. Ye, H. Ge, J. Chen, W. Liu, and Z. Liu, J. Colloid Interface Sci. **506**, 217 (2017).
[11]S. Mondal, S. Ganguly, P. Das, D. Khastgir, and N. C. Das, Compos. B: Eng. **119**, 41 (2017).
[12]S. Kuester, C. Merlini, G. M. O. Barra, J. C. Ferreira, A. Lucas, A. C. de Souza, and B. G. Soares, Compos. B: Eng. **84**, 236 (2016).
[13]G. D. Bellis, A. Tamburrano, A. Dinescu, M. L. Santarelli, and M. S. Sarto, Carbon **49**, 4291 (2011).
[14]X. Jiang, D.-X. Yan, Y. Bao, H. Pang, X. Ji, and Z.-M. Li, RSC Adv. **5**, 22587 (2015).
[15]S. H. Park, P. Thielemann, P. Asbeck, and P. R. Bandaru, Appl. Phys. Lett. **94**, 243111 (2009).
[16]J.-M. Thomassin, C. Jérôme, T. Pardoen, C. Bailly, I. Huynen, and C. Detrembleur, Mater. Sci. Eng., R **74**, 211 (2013).
[17]J.-H. Lin, Z.-I. Lin, Y.-J. Pan, C.-L. Huang, C.-K. Chen, and C.-W. Lou, Compos. B: Eng. **89**, 424 (2016).
[18]D. D. L. Chung, Carbon **50**, 3342 (2012).
[19]F. Wu, Q. Zeng, Y. Xia, M. Sun, and A. Xie, Appl. Phys. Lett. **112**, 192902 (2018).
[20]S.-T. Hsiao, C.-C. M. Ma, W.-H. Liao, Y.-S. Wang, S.-M. Li, Y.-C. Huang, R.-B. Yang, and W.-F. Liang, ACS Appl. Mater. Interfaces **6**, 10667 (2014).
[21]D.-X. Yan, H. Pang, B. Li, R. Vajtai, L. Xu, P.-G. Ren, J.-H. Wang, and Z.-M. Li, Adv. Funct. Mater. **25**, 559 (2015).
[22]J. Dalal, S. Lather, A. Gupta, S. Dahiya, A. S. Maan, K. Singh, S. K. Dhawan, and A. Ohlan, Compos. Sci. Technol. **165**, 222 (2018).

[23]W. Yang, Z. Zhao, K. Wu, R. Huang, T. Liu, H. Jiang, F. Chen, and Q. Fu, J. Mater. Chem. C **5**, 3748 (2017).
[24]F. Sharif, M. Arjmand, A. A. Moud, U. Sundararaj, and E. P. L. Roberts, ACS Appl. Mater. Interfaces **9**, 14171 (2017).
[25]H. M. Mesfin, A. C. Baudouin, S. Hermans, A. Delcorte, I. Huynen, and C. Bailly, Appl. Phys. Lett. **105**, 103105 (2014).
[26]Y. Li, B. Shen, D. Yi, L. Zhang, W. Zhai, X. Wei, and W. Zheng, Compos. Sci. Technol. **138**, 209 (2017).
[27]A. Plyushch, J. MacUtkevic, S. Svirskas, J. Banys, V. Plausinaitiene, D. Bychanok, S. A. Maksimenko, A. Selskis, A. Sokal, K. N. Lapko, and P. P. Kuzhir, Appl. Phys. Lett. **114**, 183105 (2019).
[28]B. Zhao, S. Wang, C. Zhao, R. Li, S. M. Hamidinejad, Y. Kazemi, and C. B. Park, Carbon **127**, 469 (2018).
[29]Q. Song, F. Ye, X. Yin, W. Li, H. Li, Y. Liu, K. Li, K. Xie, X. Li, Q. Fu, L. Cheng, L. Zhang, and B. Wei, Adv. Mater. **29**, 1701583 (2017).
[30]J. Liang, Y. Wang, Y. Huang, Y. Ma, Z. Liu, J. Cai, C. Zhang, H. Gao, and Y. Chen, Carbon **47**, 922 (2009).
[31]C. Lan, L. Zou, Y. Qiu, and Y. Ma, J. Mater. Sci. **55**, 6598 (2020).
[32]M. Zdrojek, J. Bomba, A. Lapińska, A. Dużyńska, K. Żerańska-Chudek, J. Suszek, L. Stobiński, A. Taube, M. Sypek, and J. Judek, Nanoscale **10**, 13426 (2018).
[33]Z. Barani, F. Kargar, K. Godziszewski, A. Rehman, Y. Yashchyshyn, S. Rumyantsev, G. Cywiński, W. Knap, and A. A. Balandin, ACS Appl. Mater. Interfaces **12**, 28635 (2020).
[34]C. Pavlou, M. G. Pastore Carbone, A. C. Manikas, G. Trakakis, C. Koral, G. Papari, A. Andreone, and C. Galiotis, Nat. Commun. **12**, 4655 (2021).
[35]P. Chamorro-Posada, J. Vázquez-Cabo, Ó. Rubiños-López, J. Martín-Gil, S. Hernández-Navarro, P. Martín-Ramos, F. M. Sánchez-Arévalo, A. V. Tamashausky, C. Merino-Sánchez, and R. C. Dante, Carbon **98**, 484 (2016).
[36]A. Tredicucci and M. S. Vitiello, IEEE J. Sel. Top. Quantum Electron. **20**, 8500109 (2014).
[37]R. Cheng, Y. Zhou, H. Liu, J. Liu, G. Sun, X. Zhou, H. Shen, Q. Wang, and Y. Zha, Opt. Mater. Express **10**, 501 (2020).
[38]A. M. Mahjoub, S. Motooka, N. Aoki, J. Song, J. P. Bird, Y. Kawano, D. K. Ferry, K. Ishibashi, and Y. Ochiai, Jpn. J. Appl. Phys., Part 1 **50**, 070119 (2011).
[39]V. Ryzhii, T. Otsuji, and M. Shur, Appl. Phys. Lett. **116**, 140501 (2020).
[40]V. Ryzhii, M. Ryzhii, V. Mitin, M. S. Shur, and T. Otsuji, J. Appl. Phys. **118**, 183105 (2015).
[41]J.-L. Coutaz, F. Garet, and V. P. Wallace, *Principles of Terahertz Time-Domain Spectroscopy* (CRC Press, 2018).
[42]N. Vieweg, F. Rettich, A. Deninger, H. Roehle, R. Dietz, T. Göbel, and M. Schell, J. Infrared Millim. Terahertz Waves **35**, 823 (2014).
[43]J. Neu and C. A. Schmuttenmaer, J. Appl. Phys. **124**, 231101 (2018).
[44]S. L. Dexheimer, *Terahertz Spectroscopy: Principles and Applications* (CRC Press, 2017).
[45]K. S. Novoselov, A. K. Geim, S. V. Morozov, D. Jiang, Y. Zhang, S. V. Dubonos, I. V. Grigorieva, and A. A. Firsov, Science **306**, 666 (2004).
[46]Z.-S. Wu, W. Ren, L. Gao, B. Liu, C. Jiang, and H.-M. Cheng, Carbon **47**, 493 (2009).
[47]J. S. Lewis, Z. Barani, A. S. Magana, F. Kargar, and A. A. Balandin, Mater. Res. Express **6**, 085325 (2019).
[48]L. Colombo, X. Li, B. Han, C. Magnuson, W. Cai, Y. Zhu, and R. S. Ruoff, ECS Trans. **28**, 109 (2010).
[49]K. F. Mak, J. Shan, and T. F. Heinz, Phys. Rev. Lett. **106**, 046401 (2011).
[50]J. Lloyd-Hughes and T.-I. Jeon, J. Infrared Millim. Terahertz Waves **33**, 871 (2012).
[51]T. Unuma, K. Fujii, H. Kishida, and A. Nakamura, Appl. Phys. Lett. **97**, 033308 (2010).
[52]R. M. Simon, Polym. Plast. Technol. Eng. **17**(1), 1–10 (1981).
[53]H. Xu, X. Yin, X. Li, M. Li, S. Liang, L. Zhang, and L. Cheng, ACS Appl. Mater. Interfaces **11**, 10198 (2019).
[54]Q. Zou, C. Shi, B. Liu, D. Liu, D. Cao, F. Liu, Y. Zhang, and W. Shi, Nanotechnology **32**, 415204 (2021).
[55]Z. Zhang, M. Zhou, T. Zhang, M. Yang, Q. Yang, J. Yu, and Y. Zhang, ACS Appl. Mater. Interfaces **12**, 19746 (2020).
[56]Y. Hernandez, V. Nicolosi, M. Lotya, F. M. Blighe, Z. Sun, S. De, I. T. McGovern, B. Holland, M. Byrne, Y. K. Gun'Ko, J. J. Boland, P. Niraj, G. Duesberg, S. Krishnamurthy, R. Goodhue, J. Hutchison, V. Scardaci, A. C. Ferrari, and J. N. Coleman, Nat. Nanotechnol. **3**, 563 (2008).
[57]M. Lotya, Y. Hernandez, P. J. King, R. J. Smith, V. Nicolosi, L. S. Karlsson, F. M. Blighe, S. De, Z. Wang, I. T. McGovern, G. S. Duesberg, and J. N. Coleman, J. Am. Chem. Soc. **131**, 3611 (2009).
[58]S. Stankovich, D. A. Dikin, R. D. Piner, K. A. Kohlhaas, A. Kleinhammes, Y. Jia, Y. Wu, S. B. T. Nguyen, and R. S. Ruoff, Carbon **45**, 1558 (2007).
[59]Z. Yan, D. L. Nika, and A. A. Balandin, IET Circuits, Devices Syst. **9**, 4 (2015).
[60]Z. Barani, A. Mohammadzadeh, A. Geremew, C. Y. Huang, D. Coleman, L. Mangolini, F. Kargar, and A. A. Balandin, Adv. Funct. Mater. **30**, 1904008 (2020).